

A CORRELATION BETWEEN GALAXY MORPHOLOGY AND Mg II HALO ABSORPTION STRENGTH

GLENN G. KACPRZAK¹, CHRISTOPHER W. CHURCHILL¹, CHARLES C. STEIDEL²,
MICHAEL T. MURPHY³, AND JESSICA L. EVANS¹

Accepted to ApJ: March 9, 2007

ABSTRACT

We compared the quantified morphological properties of 37 intermediate redshift ($0.3 \leq z \leq 1$) Mg II absorption selected galaxies to the properties of the absorbing halo gas [$0.03 \leq W_r(2796) \leq 2.90 \text{ \AA}$], observed in the spectra of background quasars. The galaxy morphologies were measured using GIM2D modeling of *Hubble Space Telescope* WFPC–2 images and the absorbing gas properties were obtained from HIRES/Keck and UVES/VLT quasar spectra. We found a 3.1σ correlation between galaxy morphological asymmetries normalized by the quasar–galaxy projected separations, A/D , and the Mg II rest–frame equivalent widths. Saturation effects cause increased scatter in the relationship with increasing $W_r(2796)$. We defined a subsample for which the fraction of saturated pixels in the absorption profiles is $f_{\text{sat}} < 0.5$. This criterion resulted in a subsample of 28 systems with $W_r(2796) \leq 1.39 \text{ \AA}$. The correlation strengthened to 3.3σ . We also find a paucity of small morphological asymmetries for galaxies selected by Mg II absorption as compared to those of the general population of field galaxies, as measured in the Medium Deep Survey. The K–S probability that the two samples are drawn from the same galaxy population is ruled out at a 99.8% confidence level. Based upon four different measures of galaxy asymmetry, it is evident that the morphological perturbations of galaxies selected by Mg II absorption are “minor” and centrally concentrated. The A/D – $W_r(2796)$ correlation suggests a connection between the processes that perturb galaxies and the quantity of gas in their halos, normalized by the impact parameter. Since the perturbations are minor, it is clear that dramatic processes or events are not required for a galaxy to have an extended halo; the galaxies appear “normal”. We suggest that common, more mild processes that populate halos with gas, such as satellite galaxy merging, accretion of the local cosmic web, and longer–range galaxy–galaxy interactions, consequently also induce the observed minor perturbations in the galaxies.

Subject headings: quasars: absorption lines—galaxies: halos—galaxies: interactions

1. INTRODUCTION

Metal–line absorbing galaxies are selected by their gas cross sections, i.e., the presence of extended, associated gaseous halos detected in quasar absorption lines. Since the kinematic, chemical, and ionization conditions of the gaseous halos can be studied in detail and compared directly to the galaxies themselves, these galaxy–absorber pairs provide insight into the role of gas in galaxy evolution. A connection between galaxy morphological characteristics and absorption properties would provide constraints on competing scenarios of the dynamics, enrichment, and geometry of halos.

The use of high spatial resolution imaging, such as WFPC–2/*HST* and ACS/*HST*, provides the opportunity to study the morphology of intermediate redshift galaxies with unprecedented detail. One of the first techniques for classifying and quantifying the morphologies of intermediate–to–high redshift galaxies is the C – A method (Abraham et al. 1994), where C is the concentration of light and A is the asymmetry of the galaxies. This technique has been applied to magnitude–limited samples in the Hubble Deep Field (Abraham et al. 1996a), the Medium Deep Survey (Abraham et al. 1996b), and the Ohio State University Bright Spiral Galaxy Survey (Whyte et al. 2002).

Simard et al. (2002) developed GIM2D, a two–dimensional decomposition fitting program that models structural param-

eters of galaxies. This program has been used to quantify the morphologies of Hubble Deep Field North galaxies (Marleau & Simard 1998), the luminosity–size relation of field disk galaxies for $0.1 \leq z \leq 1.1$ (Simard et al. 1999), the number density and luminosity function of E/S0 galaxies for $z \leq 1$ (Im et al. 2002), and the morphologies and bar structures of field galaxies at $0.4 \leq z \leq 1.1$ (Zheng et al. 2005).

Despite the availability of these tools, there has been little effort put forth toward quantifying the morphology of galaxies selected by metal–line absorption in quasar spectra. To our knowledge, there is only one study in which the morphologies of two OVI absorbing galaxies were quantified using the C – A method (Savage, Tripp, & Lu 1998). These galaxies have impact parameters $100 h_{75}^{-1}$ and $350 h_{75}^{-1}$ kpc, respectively ($q_0 = 0.05$, $\Omega_\Lambda = 0$). Based upon the concentration parameter, they find that these two galaxies are Sbc–Sc spirals. They also find that their asymmetries are lower than that of strongly interacting or irregular galaxies.

Though various classes of metal–line absorbers are available for sample selection, the Mg II $\lambda\lambda 2796, 2803$ doublet is arguably the best for studying the association of absorption with galaxies. Mg II is observable from the ground for intermediate redshifts, a regime where galaxies can be well resolved in *HST* images. Mg II absorption probes low ionization halo and is detectable in environments spanning five decades of HI column densities (Churchill et al. 2000a), from sub–Lyman limit (e.g., Churchill et al. 1999b) to damped Ly α systems (e.g., Rao & Turnshek 2000). The association of normal, bright, field galaxies with Mg II absorption at moderate impact pa-

¹New Mexico State University, Las Cruces, NM 88003
glennk@nmsu.edu, cwc@nmsu.edu, jlevans@nmsu.edu

²Caltech, Pasadena, CA 91125 ccs@astro.caltech.edu

³Institute of Astronomy, Cambridge CB3 0HA, UK mim@ast.cam.ac.uk

rameters has been well established (e.g., Bergeron & Boissé 1991; Steidel, Dickinson, & Persson 1994).

Much of our current understanding of MgII absorption selected galaxies is based upon the galaxy B and K luminosities, rest-frame $B - K$ colors, and impact parameters (Steidel, Dickinson, & Persson 1994; Churchill, Steidel, & Vogt 1996; Churchill et al. 2000b). The spectroscopic types of these galaxies have been based upon their colors from ground-based images (e.g., Bergeron & Boissé 1991; Steidel, Dickinson, & Persson 1994; Chen & Lanzetta 2003), or, in a few cases, based upon their spectra (e.g., Spinrad et al. 1993; Guillemin & Bergeron 1997). Steidel, Dickinson, & Persson (1994) determined that the average $B - K$ color for MgII absorbing galaxies is consistent with that of an Sb galaxy, though all galaxy colors redder than an Sd color are represented. Using Sloan g , r , and i band images toward 700 quasars, Zibetti et al. (2005, 2006) also find galaxy colors similar to those of local Sb-c spirals based upon statistical methods. Space-based WFPC-2/*HST* images of intermediate redshift absorption selected galaxies qualitatively reveal that their morphological types appear to be similar to those of local spiral and elliptical galaxies (Steidel 1998; Chen et al. 2001; Chen & Lanzetta 2003; Kacprzak, Churchill, & Steidel 2005; Churchill, Kacprzak, & Steidel 2005).

In the local universe, where case-by-case studies can be very detailed, the morphologies of galaxies have provided important insights for understanding the characteristics of gaseous halos. There are several case studies where faint halo gas is observed in emission to a projected distance of 13 kpc; the majority of these galaxies have either been harassed by and/or are interacting with other galaxies, as is apparent from their morphological asymmetries and HI warps (Puche et al. 1992; Swaters, Sancisi & van der Hulst 1997; Rand 2000). If local interacting or perturbed galaxies have more gas ejected into their halos, then intermediate redshift metal-line absorption selected galaxies might likewise display some evidence of morphological perturbations. If so, what can a galaxy's morphology and/or morphological perturbations tell us about the absorption characteristics of the halo gas? Moreover, what can galaxy perturbations tell us about the mechanisms that populate galaxy halos with gas?

In order to shed light on these questions, we have applied GIM2D on WFPC-2/*HST* images to quantify the morphologies of known MgII absorbing galaxies at intermediate redshifts. We aim to examine whether the morphologies of metal-line absorption selected galaxies can provide insight into the quantity and distribution of gas residing in their extended halos. We have employed several asymmetry measures, since each invokes different methods for quantifying deviations from an axisymmetric, smooth morphology. Our study has revealed a correlation between the rest-frame equivalent width of the MgII $\lambda 2796$ transition, $W_r(2796)$, and the galaxy morphological asymmetries normalized by the impact parameter, i.e., the projected galactocentric distance to the absorption.

This paper is organized as follows: In § 2, we present our sample selection methodology, the resulting sample, and the data reduction methods we employed. In § 3, the basic details of quantifying the galaxy morphological asymmetries are presented. We present our results and analyze the differences between various methods of measuring morphological asymmetries in § 4. In § 5, we discuss the implications of our analysis. Concluding remarks are provided in § 6. Through-

out this paper, we adopt a $H_0 = 70 \text{ km s}^{-1} \text{ Mpc}^{-1}$, $\Omega_m = 0.3$, and $\Omega_\Lambda = 0.7$ cosmology.

2. GALAXY SELECTION AND DATA ANALYSIS

Our sample of galaxies is selected by the presence of MgII absorption in ground-based, optical quasar spectra, primarily high resolution ($R = 45,000$, $\text{FWHM} \simeq 6 \text{ km s}^{-1}$) HIRES/Keck (Vogt et al. 1994) or UVES/VLT (Dekker et al. 2000) data. These high signal-to-noise ratio spectra provide a MgII $\lambda 2796$ rest-frame equivalent width detection threshold of $W_r(2796) \simeq 0.02 \text{ \AA}$. Thus, we have been able to select galaxies associated with a wide range of $W_r(2796)$, including the so called “weak” systems, i.e., $W_r(2796) < 0.3 \text{ \AA}$ (Churchill et al. 1999b, 2006).

In the cases where we have a HIRES or UVES quasar spectrum of an MgII absorber, we have measured the absorption properties and equivalent widths from the data. The HIRES spectra were reduced using IRAF⁴. The UVES spectra were reduced using the standard ESO pipeline and a custom code called the UVES Post-Pipeline Echelle Reduction (UVES POPLER, Murphy 2006). Analysis of the MgII absorption profiles was performed using graphic-based interactive software of our own design (Churchill et al. 1999b, 2000a; Churchill & Vogt 2001; Churchill, Vogt, & Charlton 2003) for local continuum fitting, objective feature identification, and for measuring absorption properties. For MgII absorbers where we do not have a HIRES or UVES quasar spectrum, we obtained the measured $W_r(2796)$ from the literature.

We have limited our selection of galaxies to those with spectroscopically measured redshifts that are consistent with the redshift of the MgII absorption in the range $0.3 \leq z \leq 1.0$. The galaxy redshifts are either obtained through our previous work (Steidel, Dickinson, & Persson 1994; Churchill, Steidel, & Vogt 1996; Steidel et al. 1997, 2002), or from the literature. In order to examine the galaxy morphologies, we further limited our sample to include only those galaxy-absorber pairs in quasar fields that have been imaged with either the F702W and/or F814W filter using WFPC-2/*HST*. The WFPC-2 images were obtained for various research programs and are available in the *HST* archive. The F702W filter provides a broad-band image similar to a rest-frame Johnson B -band filter for galaxies at $z \sim 0.6$. The F814W filter provides an image similar to the rest-frame B -band for galaxies at $z \sim 0.85$.

All WFPC-2/*HST* images were reduced using the WFPC-2 Associations Science Products Pipeline (WASPP⁵). The WFPC-2 astrometry is calibrated to the USNO2 Catalog (Monet et al. 1998). Offsets for combining images are performed either by cross-correlation, jitter information, and/or image world coordinate system information. Robust average images are obtained using the method of artificial skepticism (Stetson 1989), which uses a continuous weighting scheme derived directly from the data. WASPP data quality verifications include photometric and astrometric accuracy and correctly set zero-points. Galaxy photometry was

⁴ IRAF is written and supported by the IRAF programming group at the National Optical Astronomy Observatories (NOAO) in Tucson, Arizona. NOAO is operated by the Association of Universities for Research in Astronomy (AURA), Inc. under cooperative agreement with the National Science Foundation.

⁵ Developed by the Canadian Astronomy Data Centre (CADC) and the Space Telescope-European Coordinating Facility (ST-ECF): <http://archive.stsci.edu/hst/wfpc2/pipeline.html>

TABLE 1
 GALAXY–ABSORBER SAMPLE

QSO Field	z_{abs}	$W_r(2796)$	Mg II ^a	D (kpc)	ID _{gal} ^b	m_{HST}	Filter	Exp, sec	PID
Q0002+051	0.298059	0.246 ± 0.004	1	59.3 ± 0.3	1	19.96 ± 0.01	F702W	4600	Steidel/5984
Q0002+051	0.591365	0.102 ± 0.002	1	36.2 ± 0.4	1	21.24 ± 0.01	F702W	4600	Steidel/5984
Q0002+051	0.851407	1.119 ± 0.013	1	25.9 ± 0.5	1	22.34 ± 0.02	F702W	4600	Steidel/5984
Q0109+200	0.5346	2.26	2	45.1 ± 0.4	2,3	22.27 ± 0.02	F702W	1800	Disney/6303
Q0117+213	0.729075	0.244 ± 0.006	1	55.5 ± 1.1	1	21.06 ± 0.02	F702W	2008	Zuo/6115
Q0150–202	0.3887	0.58	2	60.0 ± 0.7	2,3	21.14 ± 0.01	F702W	5100	Steidel/6557
Q0229+131	0.417337	0.816 ± 0.022	1	37.5 ± 0.5	2,3	19.72 ± 0.01	F702W	5000	Steidel/6557
Q0235+164	0.5240	2.34 ± 0.05	3	12.1 ± 0.6	3	20.30 ± 0.02	F702W	600	Burbidge/5096
Q0450–132	0.493937	0.674 ± 0.026	1	50.1 ± 0.4	1	21.55 ± 0.01	F702W	2500	Steidel/5984
Q0450–132	0.493937	0.674 ± 0.026	1	62.7 ± 0.7	1	21.53 ± 0.01	F702W	2500	Steidel/5984
Q0827+243	0.524968	2.419 ± 0.017	1	37.5 ± 0.9	4	20.64 ± 0.01	F702W	4600	Steidel/5984
Q0836+113	0.7874	2.71	4	26.9 ± 0.9	5	22.63 ± 0.02	F702W	5000	Steidel/6557
Q1019+309	0.3461	0.70 ± 0.07	5	46.0 ± 0.5	1	20.47 ± 0.01	F702W	5100	Steidel/6557
Q1038+064	0.441453	0.673 ± 0.014	1	56.0 ± 0.6	6	20.70 ± 0.01	F702W	4600	Steidel/5984
Q1127–145	0.312710	1.773 ± 0.006	1	81.0 ± 0.3	2,3	19.67 ± 0.01	F814W	4400	Bechtold/9173
Q1127–145	0.312710	1.773 ± 0.006	1	45.6 ± 0.3	2,3	19.48 ± 0.01	F814W	4400	Bechtold/9173
Q1148+387	0.553362	0.644 ± 0.014	1	20.3 ± 0.6	6	20.94 ± 0.01	F702W	4800	Steidel/5984
Q1209+107	0.392925	1.210 ± 0.006	1	37.9 ± 0.4	3	21.74 ± 0.02	F702W	3600	Bergeron/5351
Q1222+228	0.550196	0.098 ± 0.009	1	36.4 ± 1.1	6	22.50 ± 0.02	F702W	5000	Steidel/5984
Q1241+176	0.550483	0.482 ± 0.013	1	21.4 ± 0.4	1	21.40 ± 0.01	F702W	5000	Steidel/6557
Q1246–057	0.639908	0.461 ± 0.006	1	29.9 ± 0.8	1	22.21 ± 0.02	F702W	4600	Steidel/5984
Q1317+277	0.660053	0.348 ± 0.007	1	103.2 ± 0.6	6	21.35 ± 0.01	F702W	4700	Steidel/5984
Q1332+552	0.3740	2.90	2	27.9 ± 0.5	7	19.40 ± 0.01	F702W	2800	Steidel/6557
Q1511+103	0.4369	0.454 ± 0.046	6	38.2 ± 0.4	2,3	21.22 ± 0.01	F702W	5000	Steidel/6557
Q1622+235	0.317596	0.491 ± 0.012	1	54.6 ± 0.5	8	19.45 ± 0.01	F702W	24,000	Steidel/5304
Q1622+235	0.368113	0.253 ± 0.008	1	114.0 ± 0.4	8	20.00 ± 0.01	F702W	24,000	Steidel/5304
Q1622+235	0.471930	0.769 ± 0.009	1	34.1 ± 0.5	8	22.27 ± 0.01	F702W	24,000	Steidel/5304
Q1622+235	0.656103	1.451 ± 0.011	1	99.6 ± 0.5	8	22.52 ± 0.02	F702W	24,000	Steidel/5304
Q1622+235	0.702903	0.032 ± 0.003	1	112.7 ± 0.9	8	21.63 ± 0.01	F702W	24,000	Steidel/5304
Q1622+235	0.797079	0.468 ± 0.009	1	71.5 ± 1.3	8	22.37 ± 0.02	F702W	24,000	Steidel/5304
Q1622+235	0.891280	1.548 ± 0.008	1	23.2 ± 0.5	8	22.65 ± 0.02	F702W	24,000	Steidel/5304
Q1623+268	0.8885	0.68 ± 0.03	7	48.2 ± 0.5	1	23.64 ± 0.03	F702W	4600	Steidel/5984
Q1623+268	0.8875	0.27 ± 0.02	7	69.9 ± 1.3	1	23.80 ± 0.06	F702W	4600	Steidel/5984
Q2128–123	0.429820	0.464 ± 0.004	1	48.8 ± 0.5	2,3	20.42 ± 0.01	F702W	1800	Mecchetto/5143
Q2206–199	0.751923	0.886 ± 0.003	1	44.2 ± 0.7	3	22.35 ± 0.01	F702W	5000	Steidel/6557
Q2206–199	0.948361	0.253 ± 0.002	1	87.2 ± 0.5	3	21.92 ± 0.01	F702W	5000	Steidel/6557
Q2206–199	1.017040	1.057 ± 0.005	1	104.6 ± 1.4	3	20.99 ± 0.01	F702W	5000	Steidel/6557

^a Mg II Absorption: (1) This paper, (2) Guillemin & Bergeron (1997), (3) Lanzetta & Bowen (1992), (4) Steidel, Dickinson, & Persson (1994), (5) Steidel & Sargent (1992), (6) Foltz et al. (1986), (7) Sargent, Bokserberg & Steidel (1988).

^b Galaxy Identification: (1) Steidel, Dickinson, & Persson (1994), (2) Bergeron & Boissé (1991), (3) Guillemin & Bergeron (1997), (4) Kanekar & Chengalur (2001), (5) Lowenthal et al. (1990), (6) Steidel et al. (2002), and (7) Miller, Goodrich, & Stephens (1987), (8) Steidel et al. (1997).

performed using the Source Extractor (SExtractor) package (Bertin & Arnouts 1996) with a detection criterion of 1.5σ above background. The m_{F702W} and m_{F814W} magnitudes were measured using the WFPC–2 zero points (Whitmore 1995), based upon the Vega system. Uncertainties in magnitudes range from 0.01 to 0.02.

Our final sample comprises 37 galaxies with magnitudes in the range $19.4 \leq m_{HST} \leq 23.8$ selected by “weak” (Churchill et al. 1999b), “classic” (Churchill et al. 2000b), and “strong” (Bond et al. 2001) Mg II absorption spanning the equivalent width range $0.03 \leq W_r(2796) \leq 2.90 \text{ \AA}$. Note that for three of the absorbers, each have two galaxies at the same redshifts. Since it is always possible that a pair of galaxies can give rise to the absorption and such conditions can provide further insights into the galaxy–absorption connection, we do not exclude these pairs from our sample.

The sample is presented in Table 1, where we list (1) the quasar field, (2) the Mg II absorption redshift, (3) the rest-frame Mg II $\lambda 2796$ equivalent width, $W_r(2796)$, and uncertainty (when available), (4) the source of quoted Mg II measurements, (5) the quasar–galaxy impact parameter, D , and uncertainty, and (6) the reference(s) for the galaxy identification. We also list (7) the apparent magnitude of the galaxy and

uncertainty as measured in the WFPC–2 filter (8), (9) the exposure time, and (10) the PI name and program identification of the WFPC–2 image. Further details about the quasar fields, the absorbing galaxies, and the absorption properties will be published in an upcoming paper (Kacprzak et al. 2007).

The impact parameters, D , presented in Table 1, are computed using the galaxy 1.5σ isophotal centroids determined by SExtractor. There is a ~ 0.05 pixel uncertainty in the position of the quasar based upon centroiding errors of unresolved sources in the images. As described below, we modeled the galaxies using GIM2D (Simard et al. 2002), which provides a second isophotal centroid. The dominant uncertainty in D is derived from the pixel offset of the galaxy isophotal center obtained using SExtractor and the isophotal center of the galaxy model determined by GIM2D. This offset is typically about 0.25 pixels.

WFPC–2 portraits of the galaxies are presented in the left-hand panels of Figure 1a. The portraits have an area 10 times larger than the 1.5σ galaxy isophotal area. The encircled arrow next to the portrait provides the direction to the quasar relative to the galaxy; also shown are the cardinal directions. The accompanying panels are the image of the GIM2D model and the residual image. These are discussed below.

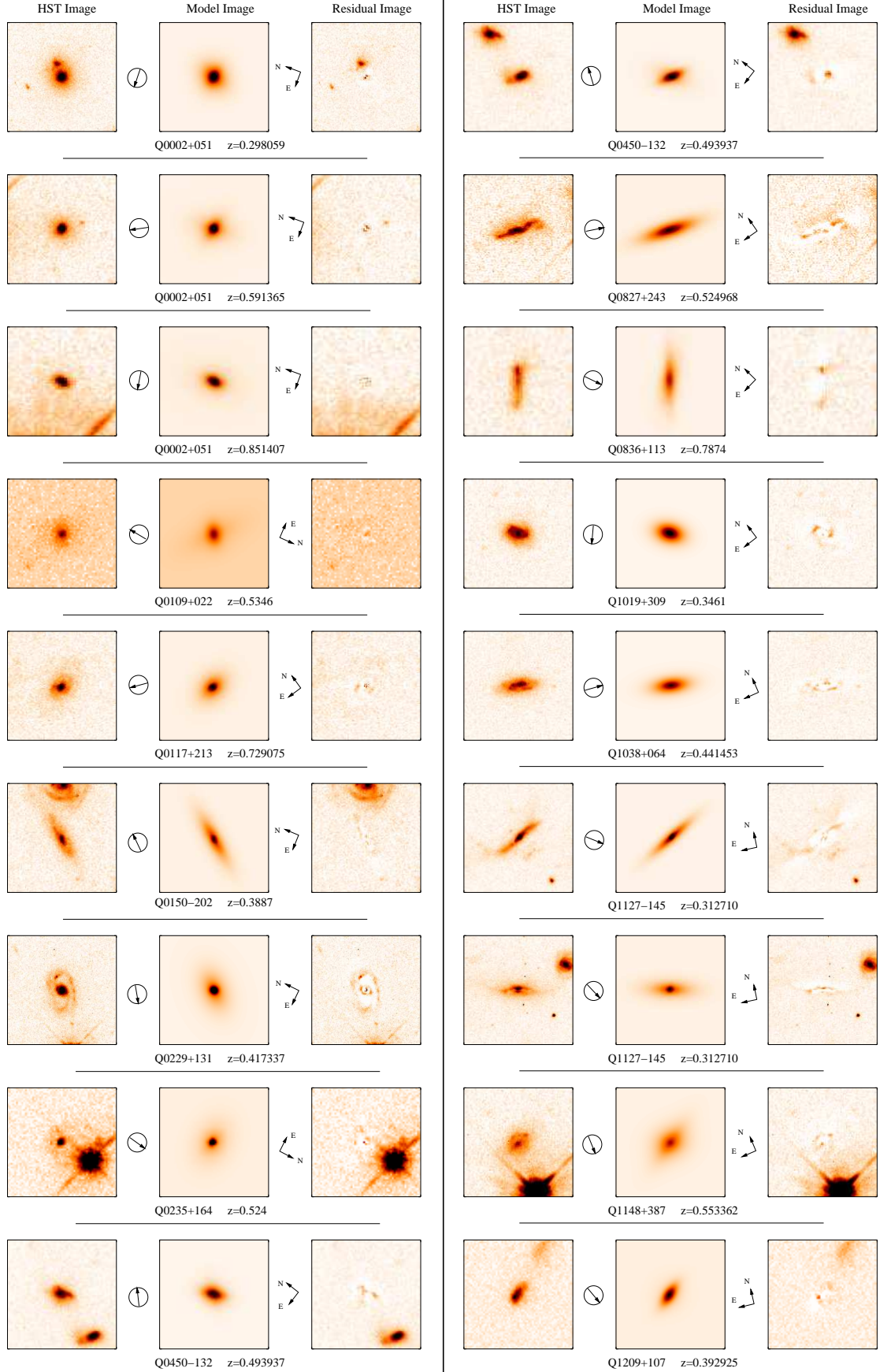
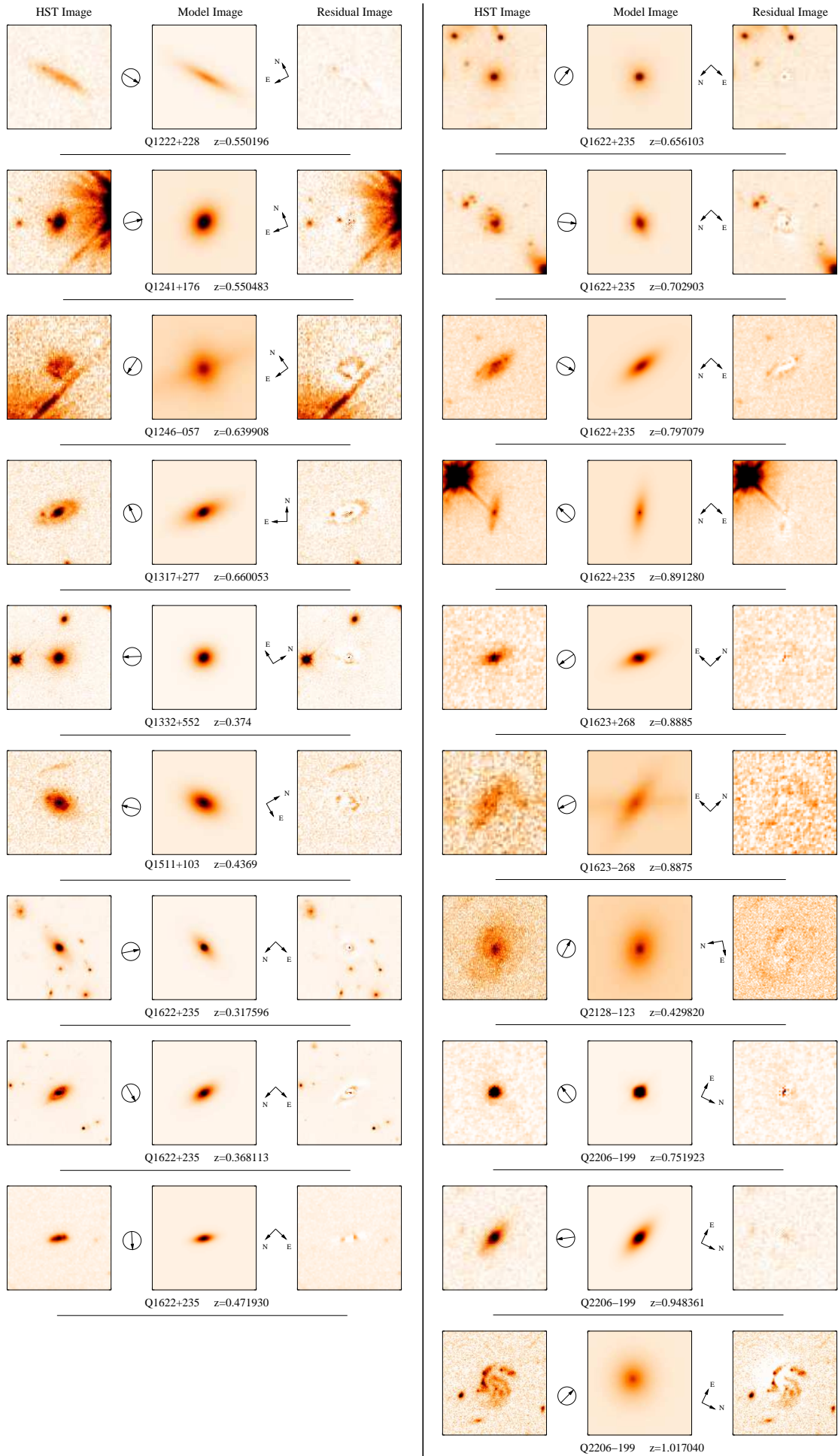


FIG. 1a.— (left) WFPC-2 images of galaxies selected by Mg II absorption. The images are 10 times larger than the 1.5σ isophotal area. — (center) The GIM2D models of the galaxies, which provide quantified morphological parameters. — (right) The residual images from the models, showing the underlying structure and morphological perturbations of the galaxies, which are quantified using various asymmetry measures. The encircled arrow provides the direction to the quasar (galaxy-quasar orientation) and the cardinal directions are shown. The quasar name and redshift of Mg II absorption is shown under each set of galaxy WFPC-2, model and residual image.



3. QUANTIFYING GALAXY ASYMMETRIES

For each galaxy, the morphology was quantified by fitting a two-component (bulge+disk) parametric model to its two-dimensional surface brightness distribution using GIM2D (Simard et al. 2002). We fitted the surface brightness of the bulge component with a de Vaucouleurs profile and the surface brightness of the disk component with an exponential profile. The centroids of the bulge and disk components are forced to be co-spatial; they are also fitted parameters. We employed this standard profile on all galaxies in our sample in order to ensure uniform parameterization. The models are convolved with the WFPC-2 point spread function, which was determined at the appropriate locations on the image using Tiny Tim (Krist & Hook 2004).

Our goal for employing GIM2D to fit *HST* galaxy images is to derive structural and morphological parameters that can be used for quantitative comparison with quantified absorption properties, primarily the MgII rest-frame equivalent width. We are particularly interested in quantified measurements of the morphological perturbations, or asymmetries in our absorption selected galaxies. GIM2D computes four measures of asymmetry using the formalism of Abraham et al. (1994), Schade et al. (1995), and Simard et al. (2002). Portraits of the GIM2D model galaxies (center panels) and the residual images (right-hand panels) are presented in Figure 1a. The residual image is obtained by subtraction of the GIM2D model image from the *HST* image. For the residuals, regions that lie outside the SExtractor segmentation image are identical to the *HST* images.

The first asymmetry measure is obtained from the *C*-*A* method of Abraham et al. (1994). The Abraham *A* is computed directly from the data (model independent) from

$$A = \frac{\sum_{ij} \frac{1}{2} |I_{ij} - I_{ij}^{180}|}{\sum_{ij} I_{ij}} - \frac{\sum_{ij} \frac{1}{2} |B_{ij} - B_{ij}^{180}|}{\sum_{ij} I_{ij}}, \quad (1)$$

where the I_{ij} are the counts at pixel ij and the I_{ij}^{180} are the counts at the ij location following a 180° rotation of the galaxy. The domain of the sums is an elliptical isophotal area defined by galaxy counts 2σ above background. The background counts, B_{ij} , are randomly selected from pixels just beyond the SExtractor segmentation image. Uncertainties in the *A* are determined by computing *A* for different random selections of the B_{ij} . In GIM2D, four realizations of background are computed. For the best value of *A*, we take the average of the four realizations and for the uncertainty in *A* we compute the standard deviation of these realizations about the average.

The second asymmetry measure is the quantity R_A (Schade et al. 1995), which is also computed using Eq. 1, except that it employs the GIM2D galaxy model residuals, R_{ij} and R_{ij}^{180} , instead of the direct counts I_{ij} and I_{ij}^{180} from the data. The domain of the sums is also model dependent. R_A is evaluated for each of the GIM2D galaxy model circular apertures, $1-10 r_h$ (half-light radii) for R_{ij} that are $1, 3$ and 5σ above background. Thus, there are 30 values of R_A representing 10 circular apertures in units of r_h for three significance thresholds. As with the Abraham *A*, the background counts are randomly selected from the pixels just beyond the SExtractor segmentation image.

Two additional methods, denoted as A_z and D_z

(Simard et al. 2002), are unique to GIM2D. Both are computed directly from the data, but using the GIM2D model circular apertures. A_z is evaluated for each of ten circular apertures, $1-10 r_h$, and is the sum of all I_{ij} having signal $2, 3$, and 5σ greater than that of the 180° symmetrical counterpart normalized by the total counts. Similar to the R_A , there are 30 values of A_z representing 10 circular apertures in units of r_h for three significance thresholds. D_z is computed exclusively outside the GIM2D model circular aperture $1 r_h$. It is the sum of all I_{ij} that are 1.5σ above background for which the symmetric counterpart I_{ij}^{180} are less than 1.5σ above background. The sum is normalized by the total galaxy total flux. D_z is a sensitive measure of highly asymmetric spiral arms, tidal tails, and highly asymmetric perturbations, since such features tend to be located to one side of a galaxy (see, for example, Q1246-057 and Q2206-199 at $z = 1.0170$ in Figure 1a). Comparing D_z to the other asymmetric measures provides insight for discriminating if a galaxy has suffered strong interactions or only slight morphological perturbations.

The WFPC-2 image exposure times range from 600 s to 24,000 s, with a typical time of 5000 s. The quantified morphological parameters obtained from the 600 s exposure (Q0235+164) should be viewed with caution. It may also be of concern that the longest exposure of 24,000 s (Q1622+235) could have different measured morphological parameters if the exposure time was of the order of 5000 seconds. To verify that the these values did not change drastically as a function of exposure time, we degraded the 24,000 s exposure to both 10,000 and 5000 s and measured the morphological parameters for these three exposure times. For all seven galaxies in the degraded 10,000 s exposure, the measured values are consistent within the uncertainties of the measurement. For the degraded image of 5000 s, the average percent difference is 9% but this is not systematic (some increase slightly, some decrease slightly). The quoted errors in the morphological parameters for the Q1622+235 field reflect the errors in the 5000 s exposure.

3.1. Effects of PSF Subtraction

Seven galaxy-absorber pairs lie at relatively small impact parameters such that the quasar light potentially contaminates the two-dimensional light profiles of the galaxies (e.g., Q0002+051 $z = 0.851407$, Q0235+164, Q0827+243, Q1148+387, Q1241+176, Q1246-057, and Q1622+235 $z = 0.891280$). In some of these cases, a diffraction spike passes through the galaxy or passes near the galaxy. In other cases, the galaxy lies within the extended tails of the complicated point spread function (PSF) illumination pattern of the quasar. Whereas galaxies far from the quasar light pattern are observed to have a uniform (flat) background, those near the quasar light pattern lie on a tilted and perhaps slightly non-uniform “background”. In some cases, there is a ramping of the background of roughly 3–5 counts over a 60 pixel radial cut toward the quasar in the vicinity of the galaxy.

In both cases, the quasar light can affect the physical boundaries of the SExtractor segmentation image and/or affect the measured morphological parameters obtained by GIM2D. We examined the effects of the quasar light contamination by performing two tests. First, when possible, we modeled and subtracted the PSF of the quasar from the image and compared the resulting segmentation images and GIM2D model parameters. Second, in cases where PSF subtraction was unsatis-

factory, we fit a two–dimension smooth surface to the slight ramping of the background (due to the quasar illumination) around a 60×60 pixel region centered on the galaxy.

In two cases (Q0827+243 and Q1148+387), the post– and pre– PSF subtracted asymmetries were consistent within the errors obtained via the four realizations of the background. In four cases (Q0002+051, Q0235+164, Q1241+176, and Q1246-057), the asymmetries differed by more than their respective background induced errors (which are inherently underestimated in that Poisson noise in the galaxy counts are not included). However, this was not a systematic effect. In two of those cases (Q0002+051 and Q0235+164) the A values increased and in two cases (Q1241+176 and Q1246-057) the A values decreased.

Due to the inherent uncertainties in PSF subtraction of saturated quasars, we adopt the A values from the pre–PSF subtracted images and use the deviations between the pre– and post– PSF subtracted images as a measure of the uncertainty in the A values. The adopted uncertainties for these seven galaxy–absorber pairs are roughly a factor of five larger than their background only induced errors.

4. ANALYSIS AND RESULTS

In Table 2, we present the quantified asymmetries for each absorption selected galaxy in our sample. In columns (1) and (2), we list the quasar field and the absorption redshift. In column (3), we list the Abraham A and uncertainty. For purposes of later discussion, we list representative values of R_A and A_z , for apertures $2 r_h$ and for 3σ and 2σ significance thresholds, respectively, in columns (4)–(5) and (6)–(7). In column (8), we list D_z .

In order to explore possible correlations between galaxy asymmetries and the strength of the absorbing gas, we performed non–parametric Spearman and Kendall rank correlation tests between the various asymmetry measures, A , R_A , A_z , and D_z , and the Mg II $\lambda 2796$ equivalent width. We also examined various scalings of the asymmetries, most notably normalization by the impact parameter, D .

For all tests, the null–hypothesis of no correlation could not be ruled out to a high level of significance (i.e., greater than 3σ), except for the Abraham A , for which a 3.1σ correlation was found between A/D and $W_r(2796)$. Recall that the Abraham A is model independent and is the only asymmetry based upon an elliptical aperture, whereas the R_A , A_z , D_z are derived from the circular model dependent apertures at various r_h . Thus, A represents a full galaxy, model independent asymmetry with a natural isophotal aperture.

At face value, the correlation between A/D and $W_r(2796)$ for the full sample (see the inset of Figure 4) suggests that, once the impact parameter of absorption is normalized out, there may be a connection between perturbations in a galaxy’s morphology and the quantity of Mg II absorbing gas probed in its halo (which is a complex distribution of column density and velocity spread). Note that for the largest equivalent widths, the scatter in A/D increases substantially. Based upon this impression, we might speculate that there is a physically based transition in the behavior of $W_r(2796)$ for large equivalent widths, i.e., a transition from a “clouds in halos” scenario to a “galactic winds” scenario [see, for example, Bond et al. (2001)]. Since absorption profiles become progressively more saturated with increasing equivalent width, it is more conservative to simply suggest that this increase in scatter could arise due to a loss of information on the quantity of gas probed by the quasar.

4.1. Equivalent Widths and Saturation

The equivalent width is a single valued measure of a complex velocity distribution of gas column density. For “weak” and “classic” systems, distinct individual clouds are usually detected with low to moderate column densities, and the number of clouds strongly correlates with equivalent width (Churchill & Vogt 2001; Churchill, Vogt, & Charlton 2003). However, for much “stronger” systems, the correlation breaks down for saturated profiles, indicating that the equivalent width can no longer be employed to accurately decipher the combination of column density, number of clouds, and their velocity distribution.

Using an approach similar to the saturation D –index employed by Ellison (2006) to efficiently pre–selected damped Ly α absorbers (DLAs), we computed the fraction saturated pixels, f_{sat} , across each HIRES or UVES Mg II $\lambda 2796$ absorption profile. The full pixel range of a profile is used, as defined using the methods of Churchill & Vogt (2001). We use the criterion that a pixel is saturated when the counts are less than $1.5 \langle \sigma \rangle$, where $\langle \sigma \rangle$ is the average of the uncertainty spectrum computed over a window $\pm 600 \text{ km s}^{-1}$ from the optical depth mean (which defines the velocity zero point). In Figure 2, we present $W_r(2796)$ versus the fraction of saturated pixels, f_{sat} . The solid points represent the galaxies in our sample for which we have HIRES and UVES spectra of the Mg II $\lambda 2796$ absorption profiles. For these data, there is some suggestion that the diagram visually breaks into four quadrants divided by $W_r(2796) \simeq 1.3 \text{ \AA}$ and $f_{sat} \simeq 0.5$. These quadrants tend to be either fully populated or entirely void of data points.

In order to ascertain whether this trend is universal to HIRES and UVES Mg II absorption profiles, we populated the figure with an additional 97 Mg II systems from our database of HIRES and UVES spectra. These systems were selected to cover the same redshift and equivalent width ranges of our sample and will be presented elsewhere as part of a larger survey (Evans et al. 2007). We plot these supplementary data as open circles in Figure 2. As can be seen, the general trend remains, especially the void of data in the quadrant defined by $W_r(2796) \leq 1.4 \text{ \AA}$ and $f_{sat} \geq 0.5$. The behavior of Mg II absorption is such that there are no profiles with a saturation fraction of $f_{sat} \geq 0.5$ and equivalent width less than $W_r(2796) \simeq 1.4 \text{ \AA}$. For equivalent widths above this value, there is a small population of profiles with $f_{sat} < 0.5$, but none of these are present in our sample.

We partitioned the $W_r(2796)$ – f_{sat} plane into four quadrants in order to objectively classify the different types of absorption profiles with the goal of defining a subsample unaffected by strong saturation. We refer to these as Q1–Q4, starting at the origin and increasing counterclockwise on the plane (Q2 is the empty quadrant). The final quadrants were determined by maximizing the number of data points in Q1 and Q3 and minimizing the number in Q2 and Q4. This method resulted in a strict equivalent width transition of $W_r(2796) = 1.39 \text{ \AA}$ and a less stringent transition of saturation in the range $0.46 \leq f_{sat} \leq 0.51$. The dashed lines on Figure 2 define the resulting quadrants, where we have adopted $f_{sat} \geq 0.5$ to designate highly saturated profiles. A Kolomorov–Smirnov (K–S) test yielded a probability of $P_{KS} < 10^{-8}$ (5.2σ) that systems with $W_r(2796) < 1.39 \text{ \AA}$ and $W_r(2796) \geq 1.39 \text{ \AA}$ are drawn from the same distribution of f_{sat} .

There are a total of nine galaxy–absorber pairs in our sample that fall into our “highly saturated” classification. For four

TABLE 2
 GALAXY ASYMMETRIES

QSO Field	z_{abs}	A	$R_A^{1\sigma, 2r_h}$	$R_A^{3\sigma, 2r_h}$	$A_z^{2\sigma, 2r_h}$	$A_z^{3\sigma, 2r_h}$	D_z^a
Q0002+051	0.298059	0.096 ± 0.0008	0.050	0.040	0.040	0.020	0.051
Q0002+051	0.591365	0.071 ± 0.0003	0.050	0.010	0.020	0.010	0.090
Q0002+051	0.851407	0.093 ± 0.011	0.090	0.040	0.010	0.000	0.220
Q0109+200	0.5346	0.041 ± 0.0053	0.042	0.016	0.013	0.000	0.236
Q0117+213	0.729075	0.079 ± 0.0018	0.060	0.050	0.010	0.000	0.130
Q0150-202	0.3887	0.095 ± 0.0012	0.058	0.052	0.069	0.028	0.075
Q0229+131	0.417337	0.089 ± 0.0008	0.080	0.070	0.050	0.030	0.060
Q0235+164	0.5240	0.210 ± 0.026	0.085	0.038	0.005	0.002	...
Q0450-132	0.493937	0.125 ± 0.0010	0.110	0.110	0.050	0.040	0.050
Q0450-132	0.493937	0.202 ± 0.0005	0.190	0.190	0.100	0.080	0.050
Q0827+243	0.524968	0.093 ± 0.0060	0.100	0.110	0.050	0.020	0.100
Q0836+113	0.7874	0.168 ± 0.0017	0.220	0.210	0.170	0.130	0.210
Q1019+309	0.3461	0.079 ± 0.0011	0.070	0.070	0.030	0.010	0.020
Q1038+064	0.441453	0.085 ± 0.0006	0.080	0.080	0.030	0.010	0.030
Q1127-145	0.312710	0.111 ± 0.0013	0.095	0.091	0.016	0.007	0.072
Q1127-145	0.312710	0.138 ± 0.0004	0.073	0.082	0.127	0.054	0.209
Q1148+387	0.553362	0.055 ± 0.0025	0.090	0.090	0.080	0.040	0.350
Q1209+107	0.392925	0.155 ± 0.0022	0.107	0.080	0.080	0.061	0.063
Q1222+228	0.550196	0.079 ± 0.0018	0.100	0.090	0.050	0.020	0.100
Q1241+176	0.550483	0.061 ± 0.012	0.050	0.020	0.060	0.030	0.100
Q1246-057	0.639908	0.122 ± 0.017	0.160	0.170	0.220	0.070	0.860
Q1317+277	0.660053	0.135 ± 0.0010	0.080	0.080	0.080	0.050	0.020
Q1332+552	0.3740	0.105 ± 0.0006	0.050	0.040	0.020	0.020	0.050
Q1511+103	0.4369	0.053 ± 0.0017	0.070	0.070	0.040	0.030	0.040
Q1622+235	0.317596	0.144 ± 0.0053	0.050	0.030	0.010	0.000	0.010
Q1622+235	0.368113	0.078 ± 0.0050	0.080	0.080	0.030	0.030	0.010
Q1622+235	0.471930	0.143 ± 0.0052	0.060	0.080	0.040	0.040	0.010
Q1622+235	0.656103	0.037 ± 0.0059	0.000	0.020	0.020	0.010	0.030
Q1622+235	0.702903	0.142 ± 0.0052	0.116	0.105	0.104	0.076	0.019
Q1622+235	0.797079	0.091 ± 0.0055	0.080	0.060	0.070	0.040	0.050
Q1622+235	0.891280	0.080 ± 0.019	0.110	0.130	0.060	0.020	0.220
Q1623+268	0.8885	0.071 ± 0.0050	0.100	0.060	0.050	0.030	0.140
Q1623+268	0.8875	0.050 ± 0.0058	0.100	0.090	0.560	0.240	...
Q2128-123	0.429820	0.036 ± 0.0029	0.036	0.042	0.021	0.009	0.250
Q2206-199	0.751923	0.202 ± 0.0002	0.135	0.035	0.061	0.062	0.036
Q2206-199	0.948361	0.089 ± 0.0017	0.064	0.041	0.009	0.002	0.043
Q2206-199	1.017040	0.306 ± 0.0024	0.460	0.530	0.430	0.310	0.670

^a The D_z computations for the galaxies Q0235+164 at $z = 0.5240$ and Q1623+268 at $z = 0.8875$ failed.

(associated with five galaxies), we have HIRES and UVES spectra and we have directly computed their f_{sat} . However, there are four in the range $2.3 \leq W_r(2796) \leq 2.90 \text{ \AA}$ for which we do not have HIRES or UVES quasar spectra (Q0109+200,

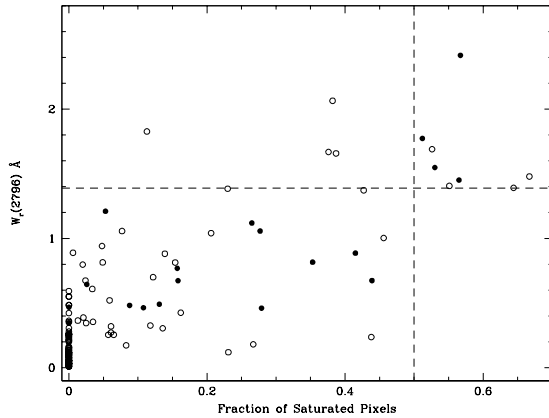


FIG. 2.— The Mg II $\lambda 2796$ equivalent width as a function of the ratio of the number of saturated pixels to total pixels, f_{sat} , for profiles observed with HIRES and UVES spectra. Both the dashed lines were obtained by maximizing the number of points in the lower left and upper right quadrants (Q1 and Q3) and minimizing the number of points in lower right and upper left quadrants (Q2 and Q4). We define a profile as highly saturated for $f_{sat} \geq 0.5$. The horizontal dashed line provides a natural and objective equivalent width transition of $W_r(2796) = 1.39 \text{ \AA}$ for defining our subsample.

Q0235+164, Q0836+113, and Q1332+552), and cannot directly compute their f_{sat} . Fortunately, the Mg II $\lambda 2796$ profiles of the absorbers in the Q0235+164 and Q0836+113 fields are available for inspection in Lanzetta & Bowen (1992) and Turnshek et al. (1989), respectively. Their spectra are of comparable resolution to HIRES and UVES. These two absorbers appear to clearly have $f_{sat} > 0.5$, indicating that they are also highly saturated. Based upon our investigation, it is reasonable to assume that the very large $W_r(2796)$ absorbers in the Q0109+200 and Q1332+552 fields also have highly saturated profiles.

4.2. Examining a Homogeneous Subsample

Applying the above motivated 50% saturation limit, which corresponds to $W_r(2796) < 1.39 \text{ \AA}$, we obtain a subsample of galaxy-absorber pairs with a higher degree of homogeneity that can be investigated in more detail for a deeper understanding of the nature of $A/D-W_r(2796)$ correlation. The subsample comprises 28 absorber-galaxy pairs from which the highly saturated profiles have been excluded. For these highly saturated profiles, the single valued equivalent width is a less reliable measure of the quantity and complex distribution of absorbing gas.

As with the full sample, we performed non-parametric Spearman and Kendall correlation tests with the computed asymmetries for the subsample of 28. In addition to the equivalent widths, we included high resolution kinematic

properties of the absorption, i.e., the velocity spread, velocity asymmetry, number of clouds (based upon Voigt profile decomposition), and the total MgII column density [see Churchill & Vogt (2001) and Churchill, Vogt, & Charlton (2003) for definitions of these quantities]. Though these kinematic quantities correlate with $W_r(2796)$ to varying degrees (only the number of clouds is statistically significant), no single kinematic quantity provides a unique description of the magnitude of absorption as measured by the equivalent width (Churchill & Vogt 2001). Interestingly, none of the kinematic absorption properties were found to correlate with the various asymmetry measures, nor with the asymmetries normalized by impact parameter. However, the significance of the A/D - $W_r(2796)$ correlation remains highly significant with a confidence level (CL) of 99.9% (a 3.33σ result that the null-hypothesis of no correlation is ruled out).

We explored the statistical behavior of the correlations between $W_r(2796)$ and all the asymmetry measures computed using GIM2D. Recall that the Abraham A is computed over an elliptical aperture defined by 2σ above background, whereas R_A and A_z are computed for circular apertures at 10 values of r_h (model dependent) and for three different levels of significance. A selected subset of our exploration is presented in Table 3. In column (1) are the tested properties. In columns (2)–(4) are the Spearman correlation coefficient, r_s , the probability, P_S , that the tested data are consistent with the null hypothesis, and the number of standard deviations, N_σ assuming the ranks are drawn from a normal distribution. In columns (5)–(7) are the Kendall τ , the probability, P_K , and N_σ . For simplicity, we will hereafter discuss the Kendall statistics.

In Table 3, we first report that there is no significant correlation (or anti-correlation) between impact parameter, D , and $W_r(2796)$ for our subsample. The equivalent width does trend toward smaller values as D increases, but the CL is 92.5% (1.8σ), which does not classify as a statistically significant departure from the null-hypothesis. However, in our exploration, we consider the possible affects of the trend between D and $W_r(2796)$.

We first focus on the asymmetry R_A for both $R_A^{3\sigma, 2r_h}$ and $R_A^{3\sigma, 3r_h}$ (3σ above background for 2 and 3 r_h , respectively). As presented in Table 3, there is a total lack of a correlation for each of $W_r(2796)$ versus $R_A^{3\sigma, 2r_h}$ and $W_r(2796)$ versus $R_A^{3\sigma, 3r_h}$ with $\tau_K = 0.07$ and 0.06 , respectively. These statistics translate to confidence levels (CL) of 40.2% and 34.5%. When the R_A are normalized by D , moderately significant correlations arise at the 98.7% (2.5σ) and 99.3% (2.7σ) CL, respectively. To investigate these results as a function of the number of r_h , we present the behavior of the CL for both $R_A^{1\sigma}/D$ and $R_A^{3\sigma}/D$ as a function of the number of half-light radii out to 5 r_h in Figure 3a. For both sensitivity thresholds, the CL scatter around $\sim 99\%$, which are moderately significant correlations. The CL for the R_A substantially decrease for 1 r_h . This is not unexpected since the R_A are computed using the model residual images; the GIM2D models have difficulties matching the surface brightness profiles in the galaxy cores, resulting in artifacts in the residual images for $r_h \leq 1$. These model dependent artifacts tend to randomize the R_A in the cores, which washes out any signal in the correlation tests.

We next list a selected correlation test for the asymmetry for $A_z^{2\sigma, 1r_h}$ (pixels 2σ greater than their symmetric counterparts within 1 r_h) and the correlation test for D_z in Table 3. As with R_A , when the A_z is normalized by D , the Kendall probability increases from a statistically insignificant CL of 79.6% (1.3σ)

TABLE 3
RESULTS OF K-S TESTS WITH $W_r(2796) < 1.39 \text{ \AA}$

Tests	Spearman			Kendall		
	r_s	P_S	N_σ	τ_K	P_K	N_σ
W_r vs. D	-0.31	0.1137	1.58	-0.24	0.0746	1.78
R_A Method (Schade et al. 1995)						
W_r vs. $R_A^{3\sigma, 2r_h}$	0.06	0.6798	0.41	0.07	0.5977	0.53
W_r vs. $R_A^{3\sigma, 3r_h}$	0.09	0.5713	0.57	0.06	0.6552	0.45
W_r vs. $R_A^{3\sigma, 2r_h}/D$	0.45	0.0181	2.36	0.33	0.0126	2.50
W_r vs. $R_A^{3\sigma, 3r_h}/D$	0.50	0.0095	2.59	0.36	0.0071	2.69
A_z and D_z Methods (Simard et al. 2002)						
W_r vs. $A_z^{2\sigma, 1r_h}$	0.23	0.2082	1.26	0.17	0.2041	1.27
W_r vs. D_z	0.03	0.8319	0.21	0.02	0.8885	0.14
W_r vs. $A_z^{2\sigma, 1r_h}/D$	0.43	0.0243	2.25	0.29	0.0324	2.14
W_r vs. D_z/D	0.13	0.5029	0.67	0.08	0.5523	0.59
A Method (Abraham et al. 1994)						
W_r vs. A	0.40	0.0359	2.10	0.28	0.0394	2.06
D vs. A	0.25	0.1889	1.31	0.20	0.1437	1.46
W_r vs. A/D	0.64	0.0008	3.36	0.45	0.0009	3.33

to a marginally significant 96.8% (2.1σ). In Figure 3b, we show the CL behavior of $A_z^{2\sigma}/D$ and $A_z^{3\sigma}/D$ as a function of the number of half-light radii out to 5 r_h . The A_z are computed directly on the data; there are no artifacts at $r_h \leq 1$ introduced by the GIM2D models. The CL of the $A_z^{2\sigma}/D$ and $A_z^{3\sigma}/D$ tests substantially decrease for increasing r_h . The correlation test for D_z and $W_r(2796)$ reveals no indication of even a slight trend (yielding $\tau_K \simeq 0.02$) even when D_z is normalized by D (yielding $\tau_K \simeq 0.08$). Recall that D_z is sensitive to the presence of tidal arms for $r_h > 1$.

The different r_h behavior of the CL for the R_A and A_z correlation tests can be explained by considering the effect of Poisson noise. R_A is sensitive to significant fluctuations about a smooth, correlated, axisymmetric model surface. As the r_h apertures increase, the Poisson fluctuations in the pixel values become relatively more important, but at a rate much slower than for that of A_z . This is because A_z is based upon differences between pixel values and the Poisson fluctuations at larger r_h apertures can wash out the significance of these differences.

The correlation test for the Abraham A with $W_r(2796)$ is also listed in Table 3. There is a moderately significant correlation between $W_r(2796)$ and A , with CL of 96% (2.1σ). We find only a weak trend between A and D (1.5σ). However, when the A are normalized by D , a significant correlation emerges with a CL of 99.9% (3.3σ). Since the A are computed within a single isophotal area, we cannot examine the behavior of A with r_h . In Figure 4, we present A/D versus $W_r(2796)$, with the dashed line showing a maximum likelihood fit.

It could be argued that the correlation between A/D and $W_r(2796)$ might be induced by the weak trend (1.8σ) between $W_r(2796)$ and D . To investigate this, we selected correlation tests of other GIM2D model galaxy parameters versus $W_r(2796)$ for which the CL from the correlation tests were similar to the tests of the asymmetries presented in Table 3. We then divided these model galaxy parameters by D and reran the correlation tests. None of the scaling tests yielded an

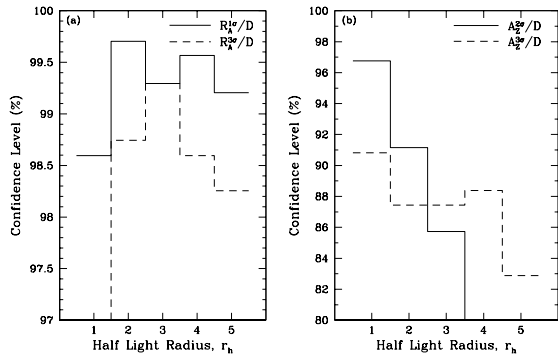


FIG. 3.— (a) Confidence level (CL) for the correlation between $W_r(2796)$ and R_A/D over the range $1 \leq r_h \leq 5$ for 1σ (solid line) and 3σ (dashed line) thresholds above background. R_A is computed from the model residual images, which are less robust near the galaxy core ($r_h \leq 1$). — (b) CL for the correlation between $W_r(2796)$ and A_z/D over the range $1 \leq r_h \leq 5$ for the 2σ (solid line) and 3σ (dashed line) cases. A_z is computed directly from the data. Both R_A and A_z employ the circular r_h apertures of the models. Note the different CL scales for panels *a* and *b*.

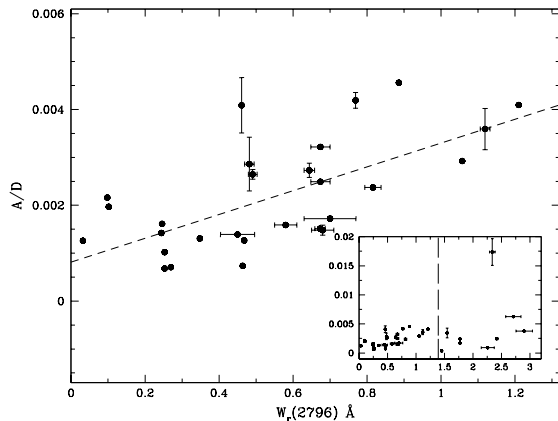


FIG. 4.— Galaxy morphological asymmetry A normalized to impact parameter, D , versus $W_r(2796)$ for the subsample with $f_{sat} < 0.5$. The error bars are 1σ ; in most cases, the errors are smaller than the data points. The correlation has a 99.92% (3.3σ) confidence level. The dashed line is a maximum likelihood fit, $A/D = 2.483 \times 10^{-3} W_r(2796) + 8.15 \times 10^{-4}$. — (inset) The same plot for the full sample, illustrating the increased scatter for larger equivalent widths. The dashed line is the cutoff for the subsample.

“induced” correlation (the highest significance was $\sim 2.0 \sigma$). In fact, in all cases where $2.0 < N_\sigma < 2.4$ prior to normalizing by D , these scaling tests yielded reduced significance.

To further investigate the confidence level we found for the $A/D-W_r(2796)$ correlation, we applied the bootstrap replacement program RESAMPLING (Howell 2004) to the subsample. We performed 10,000 bootstrapped samples, each of $n = 28$, with random replacement from the original data to determine if the correlation is due to a chance realization of the data. The bootstrap statistic corroborates the Spearman–Kendall statistics, yielding a 99% confidence level.

5. DISCUSSION

In our exploration of the morphological properties of galaxies selected by MgII absorption, we have found a statistically significant correlation (3.3σ) between the MgII $\lambda 2796$ equivalent width and galaxy asymmetry, A , normalized by the impact parameter. Background fluctuations in the calculation of A introduce only a 0.1σ spread in the significance level of the correlation. Additional uncertainties in the A values due to PSF subtraction of the quasar in the seven small impact parameter galaxy–absorber pairs (see § 3.1) introduced only a

0.2σ spread in the significance level.

It is of interest to address the individual correlation test results for A versus D and for A versus $W_r(2796)$ as presented in Table 3. First, A versus D shows a weak positive trend such that larger A are found at larger D . This suggests that uncertainty due to PSF subtraction of the quasar is not inducing elevated A values for galaxies at small D . Second, A versus $W_r(2796)$ exhibits a moderately significant correlation (2.1σ) in that large $W_r(2796)$ are associated with galaxies measured to have larger A . This hints that there may be a *direct* connection between galaxy morphological asymmetry and the quantity of gas in the galaxy halo.

However, as described above, normalization of A by D accentuates that trend, yielding a significant correlation. Therefore, for absorption selected galaxies, the $A/D-W_r(2796)$ correlation suggests a connection between the magnitude of asymmetric perturbations in a galaxy’s morphology, normalized to the galactocentric distance probed by the quasar, and the quantity of absorbing gas residing at that distance in its halo. In effect, this might be interpreted such that the influence of galaxy asymmetry diminishes with distance in a halo. The significance of the correlation is substantiated by the bootstrap replacement method. We note that this result is independent of the GIM2D galaxy models, since A is computed directly from the counts in the galaxy.

5.1. Comparison of Asymmetry Measures

The different computational details of A , R_A , A_z , and D_z render each with varying degrees of sensitivity to the details of the underlying structures that give rise to the morphological asymmetries in the galaxies. Furthermore, the relative behavior between the correlation tests provide insight for interpreting the correlation.

The CL behavior of A_z with half–light radius aperture, r_h , suggests that the tendency for a correlation of A_z/D with $W_r(2796)$ arises in the centrally concentrated region of the galaxies, primarily within $1 r_h$ (see Figure 3). In contrast, the CL behavior of R_A is fairly flat as a function of the r_h circular aperture. For larger r_h apertures, the sensitivity of R_A to asymmetries (based upon *model residuals* and the parameter r_h) may be higher than that of A_z (based upon the *data* and the parameter r_h). However, since R_A is an entirely model dependent quantity, it is not highly reliable in the central aperture ($r_h = 1$) due to difficulties with the model in the galaxy cores (yielding poor subtraction of the galaxy model in the core and thus resulting in a low CL). The low CL of D_z , which is computed exclusively outside the $r_h = 1$, suggests that the asymmetries are not due to strong spiral arms or tidal arms to one side of the galaxy (which is both consistent with the behavior of A_z and visual inspection of the galaxy images).

On the other hand, the Abraham A is an entirely model independent quantity. It is computed directly on the data over a generalized elliptical aperture defined by the region where galaxy counts are 2σ above background. Thus, the $A/D-W_r(2796)$ correlation is independent of any arbitrary assumption (such as the functional form of the bulge and disk surface brightness profiles) applied in the GIM2D modeling. Since the apertures are operationally defined using the signal–to–noise ratio of the galaxies, the asymmetries could in principle be sensitive to the pixel counts of each galaxy. The pixel counts for a given galaxy depend upon the product of exposure time and surface brightness. We calculated the signal–to–noise ratio from the surface brightness of each galaxy over their full 1.5σ aperture. A correlation test yielded no trend

between A and galaxy signal-to-noise ratio.

The combined behavior of the asymmetries and the correlation tests with r_h indicate that the asymmetries of the galaxies in our sample are centrally concentrated. The asymmetries are not the result of major perturbations that would result in significant departures from a de Vaucouleurs profile in the bulge components and an exponential profile in the disk components. As such, the morphologies of MgII absorption selected galaxies appear to be “normal” in their classifications. This suggests that extraordinary events, such as major galaxy merging or a history of galaxy harassment, are not characteristic of galaxies hosting extended gaseous halos.

5.2. Asymmetries and Absorption Selection Galaxies

Since the galaxies in our study are selected by association with MgII absorption, it is of interest to know if this selection criteria results in a population of galaxies with higher levels of morphological asymmetries (or perturbations) than the general population of magnitude selected galaxies at intermediate redshifts. The Medium Deep Survey (MDS, Abraham et al. 1996b), which employs the F814W filter, is the only survey to which we can undertake a fair comparison since the MDS galaxies have also been modeled using GIM2D and are drawn from both a similar magnitude range ($20 < m_{F814W} < 22$) and redshift range as our sample. Crampton et al. (1995) argue that the majority of galaxies in the MDS reside at $z < 1.0$ with a peak in the distribution at $z \simeq 0.6$. The range of magnitudes of our sample is $19.4 < m_{F702W} < 23.8$ and covers the redshift interval $0.3 < z < 1$ with a peak in the distribution at $z = 0.43$.

It is well known that the details of galaxy morphologies depend upon the rest-frame bandwidth in which they are observed. Almost all of the galaxies in our sample were observed with the F702W filter; only two have been observed in the F814W filter, whereas the MDS galaxies are all observed in the F814W filter. Thus, there is some concern that a quantitative comparison of asymmetries between our sample galaxies with those of the MDS may be compromised due to a non-uniform rest-frame band in which the galaxies are observed. We can only address this concern statistically. Since the peak of the redshift distribution of MDS galaxies is $z \sim 0.6$, the majority of the galaxies are observed in the rest-frame wavelength band 4530–5490 Å. For our sample, the redshift distribution peaks at $z = 0.43$, which translates to a rest-frame wavelength band of 4360–5340 Å for the majority of our sample. Therefore, there is a significant rest-frame wavelength overlap between the two samples.

Given these caveats, we performed a K–S test to examine whether the Abraham A asymmetries for the galaxies in our sample are consistent with having been drawn from the distribution resulting from the MDS survey. In Figure 5, we show the normalized distribution of A . The mode of the asymmetry distribution for our sample ($n = 37$) is highly peaked at $A = 0.08$ whereas the mode for the MDS sample ($n = 435$) is $A = 0.04$. The K–S probability that the two samples are drawn from the same A distributions is $P_{KS} = 0.0023$, which rules out the null hypothesis of similar distributions at the 99.77% confidence level (2.8σ).

This is a remarkable result given the uncertainties in the direct comparison. The dominant uncertainty is due to our lack of knowledge of the redshifts of the galaxies in the MDS sample. Abraham et al. (1996b) suggest that the extended tail in their A distribution is dominated by $z > 1$ galaxies, which are observed in the rest-frame U-band where morphological per-

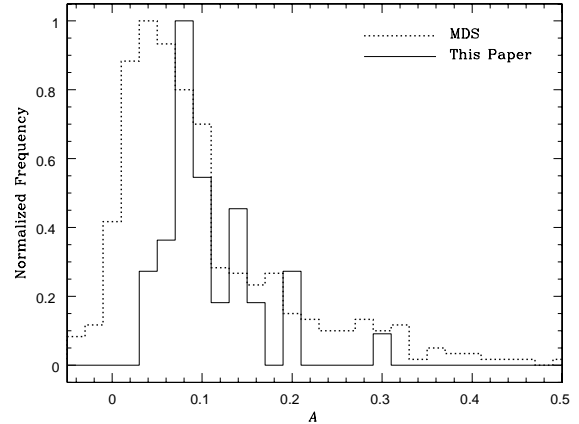


FIG. 5.— The normalized distribution of asymmetries (Abraham’s A) for the MDS (dotted line) and our sample (solid line).

turbations are significantly pronounced. Without redshifts for the MDS galaxies, we cannot select out the $z > 1$ galaxies for a more robust test. However, it is clear that the high redshift, high asymmetry tail of the MDS galaxy distribution results in a lower confidence level for the K–S test than if the tail could be objectively corrected for redshifting effects.

It is important to note that there only two MgII absorption selected galaxies with $A < 0.04$, below the mode of the MDS distribution. This constitutes only 5% of our sample. However, 29% of the A distribution for the MDS sample is populated below this value. It is the difference in this portion of the cumulative distribution function of A that dominates the K–S statistics and strongly suggests that MgII absorption selected galaxies tend to have larger morphological asymmetries than those of the galaxies in the MDS. It is quite possible that there is a bias towards galaxies with slightly larger asymmetries using MgII absorption selection.

5.3. Interpretation and Context of the Correlation

Normalizing a galaxy property by the projected distance to the quasar provides a measure of the influence the galaxy property has out to the extended regions where the gas is by chance sampled. If the influence falls off with distance, then normalizing by D provides a “scale length correction”. Our results imply that galaxy asymmetry is an important quantity for predicting the abundance of halo gas and its covering fraction and that the influence of asymmetry strengthens with proximity to the galaxy.

For local galaxies there is evidence that morphological perturbations are associated with a high covering fraction of gas beyond the visible components of the galaxies (e.g., Puche et al. 1992; Swaters, Sancisi & van der Hulst 1997; Rand 2000; Fraternali et al. 2001, 2002; Barbieri et al. 2005, also see Braun 2005). Our results for intermediate redshifts are consistent with this trend. Apparently, the greater the morphological perturbations of a galaxy, the more efficient the process of distributing gas into its halo. Furthermore, our results suggest that similar absorption strengths can arise at larger galactocentric distances from galaxies with more pronounced perturbations or at smaller galactocentric distances from galaxies with less pronounced perturbations.

Perturbations at the level measured here can be produced via minor satellite galaxy mergers with the host absorbing galaxy, mild (long range) galaxy harassment, or continued dynamical interaction with (i.e., accretion of) the local cosmic web. Satellite galaxy interactions can generate Magellanic-

type streams, increasing the gas covering factor out to ~ 50 kpc. These various mechanisms likely also gently modify the galaxy morphology and induce stochastic periods of elevated star formation (Kauffmann et al. 2006). These episodes of star formation generate galactic fountains, chimneys, superbubbles, and low-level winds (Dahlem 1997). Galaxies exhibiting negligible morphological perturbations may not have experienced these processes within the timescale that gas cycles in halos. These galaxies would be expected to produce very weak or undetectable Mg II absorption even at moderate impact parameters since they would be deficient in mechanisms that populate their halos with gas.

This scenario would explain why some bright galaxies close to the quasar produce weak absorption (Churchill et al. 2006). A natural consequence of this scenario is that it also predicts some galaxies might have such low quantities of gas in their halos that they would be excluded from an absorption selected sample even if they lie at relatively small impact parameter to a quasar. In the course of our studies, we discovered a galaxy at $z = 0.6720$ in the Q1317+274 (TON153) field at an impact parameter of $D = 58$ kpc for which the 3σ upper limit on absorption is $W_r(2796) = 0.007 \text{ \AA}$ (Churchill et al. 2007). The galaxy asymmetry is $A = 0.08$, giving $A/D = 0.0014$. This data point, though an upper limit, is consistent with expectations from the A/D - $W_r(2796)$ correlation, given the scatter of the data about the maximum likelihood fit. If the A/D - $W_r(2796)$ correlation holds true, it would be expected that “non-absorbing” galaxies have very small A/D .

The galaxy-absorber pairs for which the absorption profiles are more than 50% saturated exhibit a higher level of scatter in the A/D - $W_r(2796)$ correlation than do those that are not highly saturated. This may in part be due to the loss of information in the combined velocity spread and column density distribution of the gas in the highly saturated profiles. Our objective examination of profile saturation resulted in a natural equivalent width break of $W_r(2796) \simeq 1.4 \text{ \AA}$. This equivalent width regime may mark a true transition in the underlying physical mechanisms giving rise to the gas. Recently, we have found that galaxies selected by “weak” Mg II absorption are statistically consistent with those selected by so-called “classic” Mg II absorbers (Churchill, Kacprzak, & Steidel 2005; Churchill et al. 2006). For larger $W_r(2796)$, there is a growing body of evidence that DLAs, wind-driven galaxies, and strongly interacting galaxies are selected.

Using a statistical argument, Zibetti et al. (2006) demonstrated that galaxies selected by Mg II absorption with $W_r(2796) \geq 1.1 \text{ \AA}$ have colors consistent with star burst galaxies, whereas galaxies selected by $W_r(2796) < 1.1 \text{ \AA}$ are consistent with redder, less active galaxies. The mean color is consistent with that of an Sb spiral. Also using statistical methods, Bouché et al. (2006) reported an anti-correlation between the mass of Mg II absorbing halos and $W_r(2796)$. They argue that this correlation is inconsistent with virialized gas and suggest that a large fraction of strong Mg II absorbers galaxies [those with $W_r(2796) \gtrsim 2 \text{ \AA}$] are produced by galactic winds and/or outflows produced by active star formation. Bond et al. (2001) argue and Prochter et al. (2006) similarly suggest that Mg II absorbers with $W_r(2796) \geq 1.8 \text{ \AA}$ arise in galaxies with elevated star formation, and that the gas is likely wind driven. Nestor et al. (2006) imaged the galaxies in the fields of 15 quasars with “ultra” strong Mg II absorption [$2.7 \leq W_r(2796) \leq 6.0 \text{ \AA}$] and found that, compared to a

control sample, there is a significant excess of $L > \text{few} \times L_*$ galaxies and also possibly interacting galaxies in the quasar fields.

DLAs are also a very different environment than the Lyman-limit and sub-Lyman limit absorbers in our subsample. Highly saturated Mg II profiles with moderate velocity spreads preferentially select DLAs (Ellison 2006). It is also observed (Rao 2005) that the fraction of Mg II absorbers that select DLA environments increases with increasing $W_r(2796)$. However, it is common for DLAs to preferentially select smaller impact parameters, which would systematically elevate their A/D values.

Therefore, we can infer that absorbers with $f_{\text{sat}} < 0.5$ arise predominately from galaxies that have experienced either mild levels of interactions and/or minor mergers or ongoing accretion of the cosmic web. These processes would increase the level of star formation. The resulting asymmetry may reflect both the gravitational disturbance of the galaxy as well as surface brightness variations due to induced star formation. Absorbers with $f_{\text{sat}} \geq 0.5$ may arise predominantly from either DLAs, strong interacting galaxies, or galaxies with strong winds. If so, it would not be unexpected that active star-forming galaxies hosting winds might also adhere to the A/D - $W_r(2796)$ correlation, but with a larger scatter due to their highly saturated absorption profiles.

6. CONCLUDING REMARKS

We have examined four quantified measures of morphological asymmetries, A , R_A , A_z , and D_z in a sample of 37 Mg II absorption selected galaxies. The Mg II absorbers were selected from a database of HIRES and UVES quasar spectra, and from the literature in a few cases. We modeled the galaxies, observed with WFPC-2/HST in the F702W and F814W filters, using GIM2D. The Abraham A is model independent, whereas R_A is based upon the residuals of the GIM2D models. The A_z and D_z are computed directly from the data, but invoke apertures determined from the GIM2D models.

We report two main results:

1. We find a statistically significant correlation between the Abraham A normalized by the quasar galaxy impact parameter, D , and the Mg II $\lambda 2796$ rest-frame equivalent width. The significance is 3.1σ for our full sample of 37 galaxy-absorber pairs. However, when we limit the sample to those in which the fraction of saturated pixels in the Mg II $\lambda 2796$ absorption profiles is $f_{\text{sat}} < 0.5$, the A/D - $W_r(2796)$ correlation is significant at the 3.3σ level.
2. A Kolomorov-Smirnov test comparing the distributions of Abraham A for Mg II absorption selected galaxies and magnitude selected galaxies from the Medium Deep Survey shows the distributions are not consistent at a confidence level of 99.8%. There are caveats related to the comparison; however, the data show a clear paucity of small A for Mg II absorption selected galaxies. Selecting galaxies by absorption in quasar spectra may bias against galaxies with negligible morphological perturbations.

The A/D - $W_r(2796)$ correlation is formally statistically significant, if only at the 3.3σ level. However, it is a quite remarkable finding given the large variations in kinematic properties of Mg II absorption profiles (Churchill & Vogt 2001).

As discussed in § 5, the behavior of the correlation is consistent with a growing body of evidence that the quantity of gas in galaxy halos is connected to the processes occurring in the galaxies themselves, and that stronger, highly saturated Mg II absorbers are related to higher levels of activity.

A larger sample of galaxy-absorber pairs with both *HST* imaging data and HIRES and/or UVES quasar spectra would be instrumental for confirming and possibly strengthening the statistical significance of our results. One of the major pitfalls of studying absorption selected galaxies is that it requires intensive work to obtain a thorough census of the galaxy redshifts in quasar fields. Thus, we cannot claim that the galaxies used in this study are the only galaxies associated with the Mg II absorbers.

Our results suggest a relationship between the gaseous halo and the morphological perturbations in the host galaxy normalized to the impact parameter of the observed absorption. Further insight may be obtained by comparing the relative kinematics of the absorbing gas with those of the host galaxy. Only a half-dozen absorption selected galaxies have been studied at this level of detail (Steidel et al. 2002; Ellison et al. 2003). In addition, further exploration of correlations between C IV absorption strength and Mg II kinematics (Churchill et al. 1999a) with the galaxy morphological perturbations would provide important clues for better understanding the $A/D-W_r(2796)$ correlation. We are currently working toward these goals.

We thank Luc Simard for consultation on the details of

GIM2D modeling. We are very grateful to Wal Sargent and Michael Rauch for generously donating HIRES data for our research. We also thank Alice Shapley for expertise with PSF subtraction in WFPC-2 images. We express our gratitude to the anonymous referee for a careful reading and for insightful comments that lead to an improved manuscript. Support for this research through grant HST-AR-10644.01-A was provided by NASA via the Space Telescope Science Institute, which is operated by the Association of Universities for Research in Astronomy, Inc., under NASA contract NAS 5-26555. G.G.K acknowledges additional support from Sigma-Xi through the Grants in Aid of Research program. M.T.M thanks PPARC for an Advanced Research Fellowship. J.L.E. acknowledges support through the New Mexico Space Grant Consortium, which is administered through NASA. The imaging data presented in this paper are based on observations made with the NASA/ESA Hubble Space Telescope, obtained from the data archive at the Space Telescope Institute. STScI is operated by the association of Universities for Research in Astronomy, Inc. under the NASA contract NAS 5-26555. Some spectroscopic data were obtained at the W.M. Keck Observatory, which is operated as a scientific partnership among the California Institute of Technology, the University of California and NASA. The Observatory was made possible by the generous financial support of the W.M. Keck Foundation. Additional spectroscopic data are based on observations made with European Southern Observatory Very Large Telescope at the Paranal Observatories under various programs.

Facilities: *HST* (WFPC-2), Keck I (HIRES), VLT (UVES).

REFERENCES

- Abraham, R. G., Tanvir, N. R., Santiago, B. X., Ellis, R. S., Glazebrook, K., & van den Bergh, S. 1996a, *MNRAS*, 279, L47
- Abraham, R. G., van den Bergh, S., Glazebrook, K., Ellis, R. S., Santiago, B. X., Surma, P., & Griffiths, R. E. 1996b, *ApJS*, 107, 1
- Abraham, R. G., Valdes, F., Yee, H. K. C., & van den Bergh, S. 1994, *ApJ*, 432, 75
- Barbieri, C. V., Fraternali, F., Oosterloo, T., Bertin, G., Boomsma, R., & Sancisi, R. 2005, *A&A*, 439, 947
- Bergeron, J., & Boissé, P. 1991, *A&A*, 243, 334
- Bertin, E., & Arnouts, S. 1996, *A&AS*, 117, 393
- Bond, N. A., Churchill, C. W., Charlton, J. C., & Vogt, S. S. 2001, *ApJ*, 562, 641
- Bouché, N., Murphy, M. T., Péroux, C., Csabai, I., & Wild, V. 2006, *MNRAS*, 371, 495
- Braun, R. 2005, *ASP Conf. Ser.* 331: Extra-Planar Gas, 331,
- Chen, H.-W. & Lanzetta, K. M. 2003, *ApJ*, 597, 706
- Chen, H.-W., Lanzetta, K. M., Webb, J. K., & Barcons, X. 2001, *ApJ*, 559, 654
- Churchill, C. W., Kacprzak, G. G., & Steidel, C. C. 2005, in *Probing Galaxies through Quasar Absorption Lines*, IAU 199 Proceedings, eds. P. R. Williams, C.-G. Shu, & B. Ménard (Cambridge: Cambridge University Press), p. 24
- Churchill, C. W., Kacprzak, G. G., Steidel, C. C., & Evans, J. L. 2007, *ApJ*, in press (astro-ph/0612560)
- Churchill, C. W., Kacprzak, G. G., Steidel, C. C., & Murphy, M. T. 2006, *AJ*, submitted
- Churchill, C. W., Mellon, R. R., Charlton, J. C., Jannuzi, B. T., Kirhakos, S., Steidel, C. C., & Schneider, D. P. 1999a, *ApJ*, 519, L43
- Churchill, C. W., Mellon, R. R., Charlton, J. C., Jannuzi, B. T., Kirhakos, S., Steidel, C. C., & Schneider, D. P. 2000a, *ApJS*, 130, 91
- Churchill, C. W., Mellon, R. R., Charlton, J. C., Jannuzi, B. T., Kirhakos, S., Steidel, C. C., & Schneider, D. P. 2000b, *ApJ*, 543, 577
- Churchill, C. W., Rigby, J. R., Charlton, J. C., & Vogt, S. S. 1999b, *ApJS*, 120, 51
- Churchill, C. W., Steidel, C. C., & Vogt, S. S. 1996, *ApJ*, 471, 164
- Churchill, C. W., & Vogt, S. S. 2001, *AJ*, 122, 679
- Churchill, C. W., Vogt, S. S., Charlton, J. C. 2003, *AJ*, 125, 98
- Crampton, D., Le Fevre, O., Lilly, S. J., & Hammer, F. 1995, *ApJ*, 455, 96
- Dahlem, M. 1997, *PASP*, 109, 1298
- Dekker, H., D’Odorico, S., Kaufer, A., Delabre, B. & Kotzłowski H. 2000, *SPIE*, 4008, 534
- Ellison, S. L. 2006, *MNRAS*, 368, 335
- Ellison, S. L., Mallén-Ornelas, G., & Sawicki, M. 2003, *ApJ*, 589, 709
- Evans, J. L., et al. 2007, *ApJ*, in prep
- Foltz, C. B., Weymann, R. J., Peterson, B. M., Sun, L., Malkan, M. A., & Chaffee, F. H., Jr. 1986, *ApJ*, 307, 504
- Fraternali, F., Oosterloo, T., Sancisi, R., & van Moorsel, G. 2001, *ApJ*, 562, L47
- Fraternali, F., van Moorsel, G., Sancisi, R., & Oosterloo, T. 2002, *AJ*, 123, 312
- Guillemin p., & Bergeron, J. 1997, *A&A*, 328, 499
- Howell D., C. 2004, <http://www.uvm.edu/~dhowell/StatPages/Resampling/Resampling.html>
- Im, M., et al. 2002, *ApJ*, 571, 136
- Kacprzak, G. G., Churchill, C. W., Steidel, C. C., & Murphy, M. T. 2007, *ApJS*, in preparation
- Kacprzak, G. G., Churchill, C. W., & Steidel, C. C. 2005, in *Probing Galaxies through Quasar Absorption Lines*, IAU 199 Proceedings, eds. P. R. Williams, C.-G. Shu, & B. Ménard (Cambridge: Cambridge University Press), p. 80
- Kanekar, N., & Chengalur, J. N. 2001, *A&A*, 369, 42
- Kauffmann, G., Heckman, T. M., De Lucia, G., Brinchmann, J., Charlot, S., Tremonti, C., White, S. D. M., & Brinkmann, J. 2006, *MNRAS*, 367, 1394
- Krist, J. & Hook, R. 2004, *The Tiny Tim User Manual v6.3* (Baltimore: STScI)
- Lanzetta, K. M., & Bowen, D. V. 1992, *ApJ*, 391, 48
- Lowenthal, J. D., Caulet, A., Green, R. F., Hogan, C. J., Brown, L. W., Oliverson, R. J., & Woodgate, B. E. 1990, *BAAS*, 22, 805
- Marleau, F.R., & Simard, L. 1998, *ApJ*, 505, 585
- Miller, J. S., Goodrich, R. W., & Stephens, S. A. 1987, *AJ*, 94, 633
- Monet, D., et al. 1998, *USNO-SA2.0: A Catalog of Astrometric Standards* (Washington: US Nav. Obs.)
- Murphy, M. T. 2006, *UVES POPLER*, http://www.ast.cam.ac.uk/~mim/UVES_popler.html

- Nestor, D. B., Turnshek, D. A., Rao, S. M., & Quider, A. M. 2006, ApJ, in press (astro-ph/0610760)
- Prochter, G. E., Prochaska, J. X., & Burles, S. M. 2006, ApJ, 639, 766
- Puche, D., Westpfahl, D., Brinks, E., & Roy, J. 1992, AJ, 103, 1841
- Rand, R. 2000, ApJ, 537, 13
- Rao, S. M. 2005, in *Probing Galaxies through Quasar Absorption Lines*, IAU 199 Proceedings, eds. P. R. Williams, C.-G. Shu, & B. Ménard (Cambridge: Cambridge University Press), p. 125
- Rao, S. M., & Turnshek, D. A. 2000, ApJS, 130, 1
- Sargent, W. L. W., Boksenberg, A., & Steidel, C. C. 1988, ApJS, 68, 539
- Savage, B. D., Tripp, T. M. & Lu, L. 1998, AJ, 115, 436
- Schade, D., Lilly, S. J., Crampton, D., Hammer, F., Le Fevre, O., & Tresse, L. 1995, ApJ, 451, L1
- Simard, L., et al. 1999, ApJ, 519, 563
- Simard, L., Willmer, C. N. A., Vogt, N. P., Sarajedini, V. L., Philips, A. C., Weiner, B. J., Koo, D. C., Im, M., Illingworth, G. D., & Faber, S. M. 2002, ApJS, 142, 1
- Spinrad, H., Filippenko, A. V., Yee, H. K., Ellingson, E., Blades, J. C., Bahcall, J. N.; Jannuzi, B. T.; Bechtold, J., & Dobrzycki, A. 1993 AJ, 106, 1
- Steidel, C. C. 1995, in *QSO Absorption Lines*, ed. G. Meylan, (Springer-verlag: Berlin Heidelberg), p. 139
- Steidel, C. C. 1998, in *Galactic Halos: A UC Santa Cruz Workshop*, ed. D. Zaritsky, ASP Conference Proceeding, V136, p167
- Steidel, C. C., Dickinson, M., Meyer, D. M., Adelberger, K. L., & Sembach, K. R. 1997, ApJ, 480, 586
- Steidel, C. C., Dickinson, M., & Persson, S. E. ApJ, 437, L75
- Steidel, C. C., Kollmeier, J. A., Shapely, A. E., Churchill, C. W., Dickinson, M., & Pettini, M. 2002, ApJ, 570, 526
- Steidel, C. C., & Sargent, W. L. W. 1992, ApJS, 80, 1
- Stetson, P. B. 1989, *Advanced School of Astrophysics*, (Univerisidade de Sao Paulo), p1
- Swaters, R. A., Sancisi, R., & van der Hulst, J. M. 1997, ApJ, 491, 140
- Turnshek, D. A., Wolfe, A. M., Lanzetta, K. M., Briggs, F. H., Cohen, R. D., Foltz, C. B., Smith, H. E., & Wilkes, B. J. 1989, ApJ, 344, 567
- Vogt, S. S., et al. 1994, SPIE, 2198, 362
- Whyte, L. F., Abraham, R. G., Merrifield, M. R., Eskridge, P. B., Frogel, J. A., & Pogge, R. W. 2002, MNRAS, 336, 1281
- Whitmore, B. 1995, in *Calibrating Hubble Space Telescope: Post Servicing Mission*, eds. Koratkar A. & Leitherer, C., (Baltimore: STScI)
- Zheng, X.Z., Hammer, F., Flores, H., Assémat, F., & Rawat, A. 2005, A&A, 435, 507
- Zibetti, S., Menard, B., Nestor, D. B., Quider, A. M., Rao, S. M., & Turnshek, D. A. 2006, ApJ, in press (astro-ph/0609760)
- Zibetti, S., Ménard, B., Nestor, D., & Turnshek, D. 2005, ApJ, 631, L105